Asymmetric two-electron excitations in atomic strontium and barium

Robert P. Wood and Chris H. Greene
Department of Physics and Joint Institute for Laboratory Astrophysics, University of Colorado, Boulder, Colorado 80309-0440
(Received 18 August 1993)

We present a general nonperturbative calculation of the photoionization cross section for highly asymmetrical two-electron systems. The calculations were performed using the eigenchannel R-matrix procedure together with multichannel quantum-defect theory (MQDT), including the effects of long-range multipole interactions. The isolated-core approximation is extended to treat two-photon absorption. The calculations permit a detailed interpretation of recent experimental measurements in atomic strontium and barium.

PACS number(s): 32.80.Fb, 31.20.Di, 32.80.Dz

I. INTRODUCTION

Theoretical and experimental methods for understanding the high doubly excited states of two-electron systems have lately advanced rapidly. On the experimental side, a synchrotron radiation experiment has uncovered striking simplicity in the $^1P^o$ states of helium up to about the $N \approx 7$ ionization threshold, indicating the operation of strong propensity rules that severely limit the number of such states that can be excited from the ground state [1]. At the same time, the propensity-favored states at the highest energies exhibit strong, nonperturbative channel interactions, reflected by a complicated pattern of perturbations in the photoabsorption spectrum that has been fully understood theoretically only recently [2]. These same propensity rules were found [3] to apply to laser excitation of H^- doubly excited states from the ground state in an experiment conducted at Clinton P. Anderson Meson Physics Facility at Los Alamos (LAMPF) [4].

The extent to which these findings for He and H^- apply to doubly excited states of the alkaline-earth atoms remains unknown. Stepwise laser excitation of high doubly excited states has recently been carried out for Sr [5] and for Ba [6]. These experiments probe states in an energy range comparable to that studied in helium [1], but the excitation scheme is qualitatively different. References [5,6] excite the doubly excited states from high-ℓ Rydberg levels, which were themselves populated by a Stark-switching technique. Because these experiments begin from such a highly asymmetrical configuration, such as $6s n\ell$ in Ba, the approximate selection rules of He are believed [5] not to apply. Instead the appropriate selection rules are derived more from the fact that the "inner" valence electron is predominantly excited, as in the familiar "isolated-core excitation" (ICE) scheme.

In this paper we extend the isolated-core approximation to treat high-lying core states excited by multistep multiphoton absorption. We present the first nonperturbative calculations of the photoionization cross section as measured for Sr in Ref. [5] and for Ba in Ref. [6]. In addition to providing a confirmation of the experimental measurements, analysis of our intermediate results permits us to test the qualitative interpretations of Refs. [5] and [6] at a far more detailed level than would be possible based on the experiments alone. We find agreement with much of the interpretation presented by Eichmann *et al.* [5] and by Camus *et al.* [6], but some significant differences have also emerged, as will be apparent from Secs. III and IV below.

The theoretical description of such highly excited two-electron configurations is far from a routine task at present. A series of small-scale eigenchannel R-matrix calculations conducted in recent years [7] has demonstrated that the spectrum of all alkaline-earth atoms is well understood in the energy range near the lower ionic thresholds. At final state energies no higher than about -0.2 a.u. relative to the double-ionization threshold of each atom, reliable spectra have been obtained by solving the Schrödinger equation for both valence electrons variationally. This nonperturbative description of the electron correlation physics is typically conducted within a finite volume whose radius is in the range $r_0 \approx 20 - 50$ a.u. Escape of a single electron beyond this volume is described entirely within the framework of multichannel quantum defect theory, neglecting all channel interactions occurring at $r > r_0$.

As currently implemented, such eigenchannel R-matrix calculations would have difficulty reaching the substantially higher energies probed by the experiments of Refs. [5,6]. One reason is simply the fact that the reaction volume needs to be larger to accommodate the more diffuse ionic radial wave functions involved, leading to much larger basis sets in the variational calculation. Another limitation of those calculations [7] is more serious, however: the increasing occurrence of long-range nonperturbative channel interactions at distances far beyond the radii where exchange is important. These channel interactions derive from the near degeneracies of ionic levels. The lower ionic levels of the singly charged alkaline-earth ions have no near degeneracies between states of different orbital momenta l, because the ionic quantum defects vary strongly with l. (An exception to this statement is worth noting, namely, the fact that small ionic fine-structure splittings are present in the lighter alkaline-

earth ions. However, the channel interaction physics associated with such fine-structure splittings can be described relatively simply using routine frame transformation methods [8].) Higher-l states, on the other hand, have small quantum defects and consequently close degeneracies, which leads to strong multipole interactions out to relatively large distances that require an accurate solution of the multichannel problem beyond the size of a plausible R-matrix reaction volume. In the limit that such ionic states are *truly* degenerate in energy, which is approximately true for He^+, the "Gailitis-Damburg" transformation [9] to a "permanent dipole representation" describes the exchange of angular momenta between the two electrons out to very large distances, efficiently and analytically [10]. But the situation in the alkaline-earth atoms at higher energies is more difficult to describe, as there are *near* degeneracies rather than (virtually) exact ones. Physically, this implies that for low Rydberg states sufficiently below two nearly degenerate opposite-parity ionic levels, the spectrum will reflect the formation of a "permanent" electric dipole moment – that is, it looks permanent on the time scale of the Rydberg electron motion. However, for higher Rydberg levels a transition occurs such that eventually Rydberg levels are observed converging separately to each not-quite-degenerate ionic level having a large "induced" dipole moment (i.e., a large dipole polarizability). The transition between these two regimes of permanent versus induced dipole moments is critical for an understanding of the Sr spectra measured by Ref. [5] in particular.

In short, there is little alternative to direct solution of the close-coupling equations without exchange in the region beyond the R-matrix reaction volume, when faced with such strong long-range couplings. Various standard techniques are known to satisfactorily accomplish this direct solution, including finite difference methods and R-matrix propagation schemes. A major result of the present study is the marriage of such methods for incorporating the effects of long-range channel interactions with the eigenchannel R-matrix approach. Besides developing a numerical technique capable of accurately solving the relevant coupled differential equations at $r > r_0$, we also pursue an adiabatic representation of the long-range couplings that shows the critical ranges of energy and of radius where the channel interactions occur. The adiabatic picture is further useful in visualizing at a glance the strongest interacting channels and in spotting qualitative differences among the different alkaline-earth atoms and helium.

II. THEORETICAL PROCEDURE

The method we use is the eigenchannel R-matrix procedure together with the multichannel quantum-defect theory (MQDT). The combination of these approaches has been widely used for calculation of the photoabsorption spectra of atoms with two valence electrons Ref. [7] and more recently for carbon group atoms Ref. [11] and transition metals Ref. [12]. Although these techniques have been widely used in recent years, they have remained limited to energies near the first few ionic thresholds. The extension to higher energies has not been accomplished in earlier work, owing to the rapid increase in the number of accessible channels, and to the increasing importance of long-range multipole interactions. In alkaline-earth-metal atoms the quantum defect of the core electron will be small for high angular momenta. The outer electron can then mix these nearly degenerate orbital angular momentum states to create a "permanent" dipole moment of the core electron, and the interaction of this dipole moment with the outer electron adds a term to the Hamiltonian proportional to $1/r^2$. When the outer electron is excited to high enough Rydberg levels such that the splitting between the orbital angular momentum states is large compared to the interaction between the states the outer electron will be subjected to a new effective potential proportional to $1/r^4$.

In this section we discuss the details of the calculation. In Sec. II A we will briefly discuss the eigenchannel R-matrix approach and we will give details of our method for propagation of the wave function and its radial derivative (which is equivalent to propagation of the R matrix) through the coupling region outside of the reaction zone. The connection between the R matrix and the "smooth" short-range reaction matrix of multichannel quantum-defect theory is well known and will be given explicitly in Sec. II B. In Sec. II B, we will also discuss the calculation of transition amplitudes in the isolated-core approximation, which together with the reaction matrix comprises all of the information required to calculate the total and partial photoionization cross sections.

A. Calculation of the R matrix

We begin by describing aspects of the eigenchannel R-matrix procedure relevant to the present calculations. This method has proven to be an efficient and accurate method for calculating scattering parameters when combined with MQDT as discussed in [7].

The goal of the eigenchannel R-matrix procedure is to variationally determine a set of solutions of the time-independent Schrödinger equation. These solutions are chosen to have a constant normal logarithmic derivative everywhere on a reaction surface. For a system with two valence electrons the reaction surface is usually defined to be $r_0 = \max(r_1, r_2)$, where r_1 and r_2 are the radial distances for electron one and electron two, respectively, and r_0 is a constant box radius chosen in advance. In previous applications of the eigenchannel R-matrix procedure, the reaction volume radius r_0 was chosen large enough such that for $\max(r_1, r_2) > r_0$ the electrons could be considered to be distinguishable, and only the isotropic part of the Coulomb attraction between the escaping photoelectron and the residual ion was retained in the potential interaction. This implies that, when one of the electrons moves beyond r_0, the two electrons can no longer exchange energy or angular momentum through the $1/r_{12}$ interaction.

Inside the reaction volume the Hamiltonian for the

two-electron system is taken to have the same form as in [8]:

$$H = T_1 + T_2 + V(r_1) + V(r_2) + V_{\text{s.o.}}(r_1) + V_{\text{s.o.}}(r_2) + \frac{1}{r_{12}}, \quad (1)$$

where T_i is the kinetic energy operator for electron i. The one-electron potential $V(r_i)$ is the effective electron-core potential for electron i, which models the screening of the nuclear charge Z by the core electrons and the polarizability of the core electrons. The form of the potential $V(r_i)$ is chosen to be the same as in [7]. However, it has been pointed out that the final spectra are generally insensitive to the actual form of the potential chosen [13]. The most important point is that the one-electron energy levels of the positive ion must agree with the experimental levels. In the present calculations we have used the experimental ionic energy positions in the R-matrix calculation as well as in the MQDT calculation. The spin-orbit interaction between the nucleus and electron i is given by $V_{\text{s.o.}}(r_i)$ and is given explicitly by Eq. (3) of Ref. [7]. The electron-electron repulsion between the two valence electrons is $1/r_{12}$.

The one-electron orbitals we used in constructing our two-electron basis functions were chosen to be eigenfunctions of the one-electron Hamiltonian, specifically

$$[T_i + V(r_i) + V_{\text{s.o.}}(r_i)]|n_i(sl_i)j\rangle = E_{nlj}|n_i(sl_i)j\rangle. \quad (2)$$

Here the quantum numbers s, l_i, and j_i are respectively the one-electron spin, orbital and total angular momenta, while the principal quantum number n_i is an index that labels the one-electron eigenfunctions with the same l_i and j_i. Each one-electron orbital that is nonzero on the reaction surface $r = r_0$ is called an "open-type" orbital, while each that vanishes at r_0 is called "closed-type." The majority of the two-electron basis functions included in the R-matrix calculation are composed of two "closed-type" one-electron radial functions. Open-type orbitals are included in every channel to be treated as either open or weakly closed in the MQDT calculation.

The eigenchannel R-matrix procedure requires the solution to a generalized eigenvalue equation $\underline{\Gamma}Z = b\underline{\Lambda}Z$ at each desired energy E. The matrices $\underline{\Gamma}$ and $\underline{\Lambda}$ are defined in Ref. [7], Eqs. (7) and (8), and b is the normal logarithmic derivative constant over the reaction surface. The matrix $\underline{\Gamma}$ involves the energy, the Hamiltonian, and the Bloch operator, while the matrix $\underline{\Lambda}$ contains surface amplitudes of the basis. In Ref. [14] a streamlined method for solving the generalized eigenvalue equation was developed which greatly increased the efficiency of the eigenchannel R-matrix method. The number of nontrivial solutions to the generalized eigensystem is N_o, the number of open or weakly closed channels. We are guaranteed to have N_o solutions by including an open-type orbital in all open or weakly closed channels. The βth eigenstate of the Hamiltonian $|\psi_\beta\rangle$ is constructed from the eigenvectors $Z_{k\beta}$ as $|\psi_\beta\rangle = \sum_k |y_k\rangle Z_{k\beta}$. Here the $|y_k\rangle$ are two-electron basis functions, and the label k represents the set of quantum numbers $\{n_1 l_1 j_1 n_2 l_2 j_2\}$. The unsymmetrized two-electron basis functions have the following form:

$$|n_1(l_1 s_1)j_1, n_2(s_2 l_2)j_2\rangle \quad (3)$$

in jj coupling. At this point the normal procedure is to match the projection of the βth independent solution on the ith channel function and its radial derivative to a linear combination of regular and irregular Coulomb functions (f_i, g_i). From this matching procedure the "smooth" reaction matrix $K_{ii'}$ of MQDT is determined. This procedure neglects the effects of all higher long-range multipoles beyond the matching radius r_0. However, for the highly excited core states we are considering the electrons are able to exchange energy and angular momentum to large radial distances, approximately 100–300 a.u. This will be taken into account by numerically propagating the R matrix through this exterior region of channel coupling.

After completing the eigenchannel R-matrix calculation, we now have N_o solutions ψ_β and N_o normal radial derivatives ψ'_β on the reaction surface. Outside this surface, $r_2 > r_0$, the βth independent solution at an energy E is given by a close-coupling-type expansion, with coefficients $F_{i\beta}(r_2)$ which depend on r_2

$$\psi_\beta = \sum_{i=1}^{N_o} \Phi_i(\Omega) F_{i\beta}(r_2), \quad (4)$$

$$\psi'_\beta = \sum_{i=1}^{N_o} \Phi_i(\Omega) F'_{i\beta}(r_2). \quad (5)$$

$\Phi_i(\Omega)$ is a close-coupling-type channel function, with Ω representing all spatial and spin coordinates for the electron pair except the radial coordinate of the outer electron. The outer electron spin is ignored in the jK-coupling case. In this paper we will use either LS coupling or jK coupling. The exact form for the $\Phi_i(\Omega)$ in each coupling scheme is

$$\Phi_i(\Omega) = \chi_i(r_1)|(l_1 l_2)L(s_1 s_2)SJM\rangle, \quad (6)$$

$$\Phi_i(\Omega) = \chi_i(r_1)|(s_1 l_1)j_1 l_2 K\rangle, \quad (7)$$

with the $\chi_i(r_1)$ a radial core function for the inner electron. Here we have chosen to represent the angular momentum and spin degrees of freedom in the bra-ket notation, while using wave functions for the radial coordinate. Another point worth mentioning is that exchange effects are completely neglected in all calculations of this paper, which is the reason there is no explicit antisymmetrization in Eqs. (4) and (5).The $N_o \times N_o$ matrices $F_{i\beta}(r)$ and $F'_{i\beta}(r)$ are determined at r_0 by taking the projection of the ith channel function $\Phi_i(\Omega)$ on the βth independent solution

$$F_{i\beta}(r_0) = \langle\langle \Phi_i | \psi_\beta \rangle\rangle, \quad (8)$$

$$F'_{i\beta}(r_0) = \langle\langle \Phi_i | \psi'_\beta \rangle\rangle. \quad (9)$$

Here the double brackets refer to a surface integral over the reaction surface, which is interpreted to include also a trace over spin degrees of freedom.

If we insert Eq. (4) into the time-independent Schrödinger equation and project from the left with

$\langle\Phi_j(\Omega)|$ we arrive at the following finite set of coupled differential equations for the $F_{i\beta}(r)$:

$$F''_{i\beta}(r_2) + 2\sum_{j=1}^{N_o}[\varepsilon_i\delta_{ij} - V_{ij}(r_2)]F_{j\beta}(r_2) = 0. \quad (10)$$

Here $\varepsilon_i = E - E_i$ is the asymptotic photoelectron energy in channel i. E is the total energy and E_i is the energy of the ith core level. The potential matrix V_{ij} is given explicitly by

$$V_{ij}(r_2) = \left(\frac{l_i(l_i+1)}{2r_2^2} - \frac{Z-1}{r_2}\right)\delta_{ij} + \sum_{k=1}^{\infty}\langle\Phi_i(\Omega)|r_1^k P_k(\cos\theta_{12})|\Phi_j(\Omega)\rangle r_2^{-k-1}, \quad (11)$$

where we have neglected the effect of the spin-orbit interaction $V_{\text{s.o.}}(r_2)$ for electron 2 at $r_2 > r_0$. Equation (10) includes some closed channels i at any given energy E in which the components of $F_{i\beta}$ diverge exponentially asymptotically. The physical boundary conditions at $r \to \infty$ are applied to the $F_{i\beta}$ with the aid of quantum-defect theory, after the solutions have been propagated to radial distances sufficiently large that the long-range multipole potentials, primarily the dipole term, are of negligible importance. A multichannel Numerov algorithm was used in propagating the solution matrix $F_{i\beta}$ and its derivative $F'_{i\beta}$.

B. Calculation of the MQDT parameters

We have determined an $N_o \times N_o$ solution matrix $F_{i\beta}$ and its radial derivative $F'_{i\beta}$ from the R-matrix procedure outlined in the preceding section. We will now use these matrices to calculate the necessary MQDT parameters for calculation of the total and partial photoionization cross sections. We must determine the reaction matrix $\underline{K}$ or the scattering matrix $\underline{S}$. These matrices are functions of the energy E and give detailed information of the final state channel interactions. In this paper we will deal with the reaction matrix $\underline{K}$ but this contains equivalent information to the scattering matrix, and the two are related by a simple transformation $\underline{K} = -i(\underline{S}-1)(\underline{S}+1)^{(-1)}$ (Ref. [8]). We choose to use the reaction matrix because it is a real quantity, whereas the scattering matrix is complex.

The calculation of the reaction matrix from the solution matrices $F_{i\beta}$ and $F'_{i\beta}$ is now straightforward. For r_2 large enough that the $k \geq 1$ terms of the potential matrix V_{ij} are negligible, we see that the $F_{i\beta}$ satisfy the radial Schrödinger equation with a purely Coulomb potential in each channel i. These $F_{i\beta}$ can be matched to a linear combination of regular and irregular Coulomb functions $f_i(r)$ and $g_i(r)$ which are a function of the photoelectron energy ε_i and the orbital angular momentum l_i in channel i. This matching can be performed at any radius r_f such that the $\sum_k$ contribution to V_{ij} in Eq. (11) is negligible. The coefficients of the expansion will then be independent of r_2 and we can write

$$F_{i\beta}(r_2) = f_i(r_2)I_{i\beta} - g_i(r_2)J_{i\beta}, \quad (12)$$

$$F'_{i\beta}(r_2) = f'_i(r_2)I_{i\beta} - g'_i(r_2)J_{i\beta}. \quad (13)$$

Solution of this system of equations for the energy dependent matrices $I_{i\beta}$ and $J_{i\beta}$ yields the reaction matrix $\underline{K} = \underline{J}\,\underline{I}^{-1}$. Equivalently we could form the $\underline{R}$ matrix from the solution matrices $\underline{R} = \underline{F}(\underline{F}')^{-1}$ with the $\underline{K}$ matrix given in terms of the $\underline{R}$ matrix by

$$\underline{K} = (f - f'\underline{R})(g - g'\underline{R})^{-1}. \quad (14)$$

Here the Coulomb functions (f, g) and their radial derivatives, all evaluated at the outermost matching radius r_f, are arranged in diagonal matrices.

We have not applied the physical boundary conditions in the calculation of the reaction matrix $\underline{K}$. These boundary conditions are efficiently imposed using multichannel quantum-defect theory. We require that the wave function goes to zero in each asymptotically closed channel. Physically this boundary condition represents the fact that an electron can only escape to $r \to \infty$ in the channels i for which $\varepsilon_i = E - E_i > 0$. Therefore the number of physical solutions and any given energy E are exactly equal to the number of open channels. We form these physical solutions by taking a linear combination of the Ψ_β with the requirement that in each closed channel the wave function must go to zero. The specifics of this procedure are given elsewhere [15]; here we just note that the effect of the channel elimination is to give a highly energy dependent physical reaction matrix $\underline{K}^{\text{phys}}$ containing only indices referring to the physical channels. The strong energy dependence is caused by the infinite number of Rydberg autoionizing resonances in *every* channel; each such resonance causes a pole in $\underline{K}^{\text{phys}}$.

Along with the reaction matrix we must calculate a set of transition amplitudes which connect the initial state to the final state. To this end we use the so-called "isolated-core approximation" [16,17]. We assume that the initial state can be written as a simple product wave function. In this approximation the initial state MQDT wave function can be written as $\Psi_0 = \Phi_0(\Omega)u_{n_0l_0}(r_2)/r_2$. Here Φ_0 is a core function for the initial state with Ω representing all spatial and spin coordinates for the two electron system *except* the outer electron radial coordinate r_2. The initial state radial wave function is $u_{n_0l_0}(r_2) = r_2R_{n_0l_0}$, with $R_{n_0l_0}$ a hydrogenic wave function for the outer Rydberg electron and n_0, l_0 being the principal quantum number and the orbital angular momentum, respectively. Approximating the initial state wave function as a simple product neglects exchange and all correlation effects for the initial state; this approximation should be valid for the high l_0 values considered here, but it will be discussed further in Sec. III in the context of specific results. Outside the reaction volume the final state MQDT wave function will be as in Eq. (4) with $F_{i\beta}$ having its asymptotic form, Eq. (12). The transition amplitude connecting the initial state to the final state can then be written in general as Eq. (14) of Ref. [17]

$$D_\beta = \langle \Psi_\beta | T | \Psi_0 \rangle \tag{15}$$

$$\cong \sum_i \langle \Phi_i | T | \Phi_0 \rangle \int_{r_0}^{\infty} dr_2 [f_i(r_2) I_{i\beta} - g_i(r_2) J_{i\beta}] \times u_{n_0 l_0}(r_2) + D_\beta^{\text{inside}}. \tag{16}$$

Here we have made the standard isolated-core approximation that the transition operator T only acts on the core electron because the outer electron spends most of its time far from the nucleus where it cannot absorb visible or uv photons. D_β^{inside} is the contribution to the transition amplitude from inside of the reaction volume. The specific form of the transition operator T depends on the details of the excitation scheme, as will be discussed in more detail in Sec. III. The overlap integral of the outer electron wave function in Eq. (16) can be evaluated by applying Green's theorem, Eq. (16) of Ref. [17]

$$\int_{r_0}^{\infty} dr_2 [f_i(r_2) I_{i\beta} - g_i(r_2) J_{i\beta}] u_{n_0 l_0}(r_2) \tag{17}$$

$$= n_0^2 \nu_i^2 W(f_i(r_0) I_{i\beta} - g_i(r_0) J_{i\beta}, u_{n_0 l_0}(r_0)) / (\nu_i^2 - n_0^2). \tag{18}$$

Here $W(F,G) = FG' - F'G$ is the radial Wronskian, and ν_i is the effective quantum number in channel i.

In Ref. [17] this equation was further simplified by assuming that the energy dependence of the f and g functions could be ignored. This is a very good approximation when r_0 is small provided $\nu_i \gg l_i$. In Ref. [17] the value r_0 was taken to be 20 a.u., whereas for our calculations r_0 will be in the range of 100–250 a.u. Therefore we numerically calculate the Wronskian at each energy E.

With the MQDT parameters $\underline{K}$ and the transition amplitudes D_β we can calculate physical observables such as the partial and total cross sections efficiently through straightforward manipulations. Specifics of the procedure are given in Ref. [15].

III. RESULTS

We will now apply the formalism developed in Sec. II to calculate photoionization cross sections for strontium and barium, emphasizing the different approximations we have used for the two calculations. We will also compare our calculations with recent experimental data.

A. Photoionization cross section of strontium

In this section we give specific details for the calculation of the photoionization cross section of strontium. We will focus on the global structures in the cross section and not on a line by line comparison between the calculation and the experiment due to the enormous complexity of the spectra.

In the recent experiment of Eichmann *et al.* [5], highlying doubly excited states of strontium were probed by multiphoton excitation. The final states probed in the experiment were in the energy region near the $6f$ threshold of Sr^+ and the "initial state" was the $5d_{5/2} n_{2_i} = 17 l_{2_i} = 9$ state. This autoionizing state has such a long lifetime that we can treat it as though it is a bound level. Here the quantum number n_{2_i} is the principal quantum number for the outer electron and l_{2_i} is its orbital angular momentum for the outer electron.

As is discussed in Sec. II we have neglected exchange and correlation effects for the initial state in our calculation. This should be a very good approximation because the extremely high orbital angular momentum of the outer electron prohibits it from penetrating into the region where the inner electron wave function is large. We perform the calculation in LS coupling because the fine-structure effects are of negligible importance for the final state. Also, the total spin does not play a role in the calculation because we are neglecting exchange, so the channels are specified by the quantum numbers l_{1_i}, l_{2_i} which couple to form a total angular momentum L_i.

The experiment claimed to select a single l_{2_i} angular momentum eigenstate, but there is no knowledge of the total orbital angular momentum for the two electrons $\boldsymbol{L}_i = \boldsymbol{l}_{1_i} + \boldsymbol{l}_{2_i}$. Camus *et al.* [19] point out that more than one l_{2_i} eigenstate may be produced, but we continue in our analysis to neglect this Stark-induced mixing. We assume that the experiment incoherently excites all possible initial angular momenta L_i with equal weight. There does not seem to be any inherent reason to prefer equal weighting to a statistical weighting. Our lack of precise knowledge of the detailed preparation of the "initial state" is perhaps the greatest uncertainty in the calculations. For the initial state considered here with $l_{1_i} = 2$ and $l_{2_i} = 9$ the possible values of the total angular momentum of the initial state are $L_i = 7 \to 11$. In treating the "initial state" in LS coupling we have neglected the approximately 87 cm^{-1} fine-structure splitting of the $5d_j$ levels. However, we use the correct $5d_{5/2}$ ionic energy level in the calculation, and the initial state energy is taken to be $E_{5d_{5/2}} - 1/(2n^2)$, with $n = 17$.

The possible final states accessible by a one-photon transition are those having total final angular momentum in the range of $L_f = 6 \to 12$, with the even parity. We must do a separate calculation for each allowed initial and final state. For each possible L_i there are three possible $L_f = L_i - 1, L_i, L_i + 1$, which leads to a total of 15 MQDT calculations.

In the energy region near the $6f$ threshold we have included the following nearby thresholds in the calculation: $7d, 8p, 6f, 6g, 6h$. We use experimental threshold energies [6] in the R-matrix and MQDT calculations. For example, the R-matrix and MQDT calculation for $L_f = 12$ included the following open and weakly closed channels:

$$7d\varepsilon 10, 7d\varepsilon 12, 8p\varepsilon 11, 6f\varepsilon 9, 6f\varepsilon 11, 6g\varepsilon 8, 6g\varepsilon 10, 6g\varepsilon 12, 6h\varepsilon 7, 6h\varepsilon 9, 6h\varepsilon 11. \tag{19}$$

Here our notation is $n_{1_f} l_{1_f} \varepsilon l_{2_f}$ with the ε representing the energy of the outer electron. The channels with $l_{2_f} \geq 13$ have been found to be unimportant, and are neglected in the calculations.

The calculations were performed with an R-matrix box size of 100 a.u. and the solutions were propagated beyond this box out to radial distances of approximately 250 a.u. using the methods discussed in Sec. II. The core-electron transition amplitude Eq. (16) for a single photon excitation of the initial state $(l_{1_i}l_{2_i})L_i$ to the final state $(l_{1_f}l_{2_f})L_f$ is given by [18]

$$\langle (l_{1_i}l_{2_i})L_i||r^{(1)}||(l_{1_f}l_{2_f})L_f\rangle = C\delta_{l_{1_i}l_{1_f}}(-1)^{l_{2_i}+L_f+1}[l_{1_i}][l_{1_f}][L_f][L_i]\begin{pmatrix} l_{1_i} & 1 & l_{1_f} \\ 0 & 0 & 0 \end{pmatrix}\begin{Bmatrix} l_{1_i} & L_i & l_{2_i} \\ L_f & l_{1_f} & 1 \end{Bmatrix}. \quad (20)$$

Here we have used the convention that $[L] = \sqrt{2L+1}$. The quantity in parentheses is a Wigner 3-j symbol and the quantity in braces is a 6-j symbol. Here C is the radial matrix element of the dipole operator which is a constant. The reaction matrix was determined at $r_0 = 250$ a.u. at 2000 energy points in the energy region of 76 015–76 893 cm^{-1} above the first ionization potential. Using standard MQDT procedures we have calculated the cross section from the reaction matrix and the transition amplitudes.

In Fig. 1 we compare the relative experimental photoionization cross section with the relative theoretical cross section of the $5d_{5/2}n_{2_i} = 17l_{2_i} = 9$ state of Sr from Ref. [5]. We have modeled the saturation of the experimental cross section by plotting the theoretical cross section as $\sigma_{\rm sat} = 1 - e^{-\phi\sigma}$ (Ref. [16]). The theoretical cross section is a combination of the 15 individual cross sections $\sigma(L_i \rightarrow L_f)$, summed over L_f and L_i, which is only approximate as discussed above. While the spectrum is very complicated, we have clearly achieved qualitative and even semiquantitative agreement with the experimental cross section.

Below the $6f$ threshold which is located at approximately 23 560 cm^{-1} the spectra are very complicated due to the interaction between the $6f\varepsilon l_{2_f}$, $6g\varepsilon' l'_{2_f}$, and $6h\varepsilon'' l''_{2_f}$ Rydberg series. In this energy region these channels are closed and the Rydberg series converging to the $6f$ threshold are perturbed by the lower members of the $6g\varepsilon' l'_{2_f}$ and $6h\varepsilon'' l''_{2_f}$ series. Also, in both the theoretical and experimental cross sections there is a sudden transition below approximately 23 450 cm^{-1} where the Rydberg series converging to the $6g$ threshold are much less intense. This is at an effective quantum number ν of approximately 20 relative to the $6g$ threshold. The reason that the transition region occurs near $\nu \approx 20$ can be understood by examining the relevant frequency scales of the Rydberg electron. The outer Rydberg electron oscillates with a frequency $\omega \approx 1/\nu^3$. The energy splitting between the nearly degenerate $6g$ and $6h$ ionic thresholds introduces another characteristic frequency, which can be viewed qualitatively as the precession frequency of a near-Keplerian elliptical orbit. For Rydberg frequencies $\omega \lesssim E_{6h} - E_{6g}$ the outer electron is subjected to a dipole potential proportional to $1/r^4$, whereas for $\omega \gtrsim E_{6h} - E_{6g}$ the potential is proportional to $1/r^2$. The transition region should occur for energies $\omega \approx E_{6h} - E_{6g}$; this translates into effective quantum numbers of $\nu \approx 17$, which is close to the observed transition at $\nu \approx 20$.

One very noticeable discrepancy is seen in the region between the $6f$ and $6g$ threshold. The Rydberg series in the theoretical cross section converging to the $6g$ threshold does not match up with the experimental cross section. We have found that the agreement between theory and experiment is improved dramatically if the theoretical wavelength is shifted by $+10$ cm^{-1}. The source of this error has not been identified, the most likely problem being in the theoretical thresholds used in the MQDT. There is some disagreement about the true (experimen-

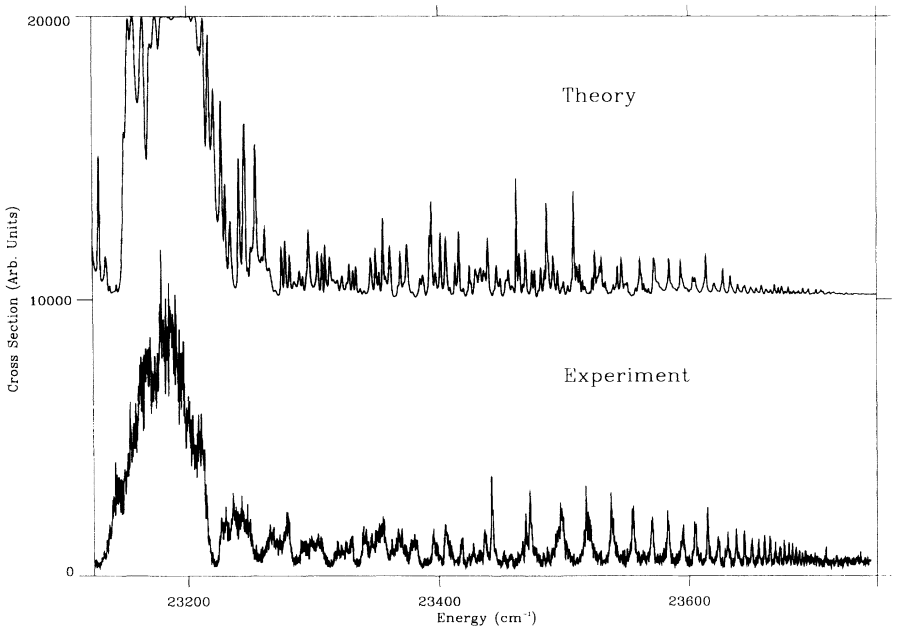

FIG. 1. Comparison of the experimental relative cross section of Ref. [10] with the present calculation. The energy of the $6f$ threshold is approximately 23 560 cm^{-1} and the nearly degenerate $6g$ and $6h$ thresholds are located at approximately 23 740 cm^{-1}.

tal) thresholds for Sr^+, as is evident from the analysis of Ref. [5].

In Fig. 2 we display a plot of the individual L_f cross sections that were included in calculating Fig. 1. Only one initial state L_i is plotted for each L_f because only the intensities change for different L_i and not the resonance positions. These figures show the rich number of features in the spectrum, many of which are not experimentally resolved.

In all of the calculations there appears one dominant Rydberg series converging to the $6g$ threshold which can be labeled $6g\varepsilon l_{2_f}$. The dominant decay path for the $6g\varepsilon' l_{2_f}$ channel is to the $6f\varepsilon l'_{2_f}$ channels. We expect the probability for the $6g\varepsilon' l_{2_f} = 8$ channel to decay into the $6f\varepsilon l_{2_f} = 9$ channel should be larger than the probability for the $6g\varepsilon' l_{2_f} = 10$ channel due to the propensity for the autoionizing electron to gain energy and angular momentum in the decay process. To verify this propensity rule we have examined the scattering probability for the processes $6g\varepsilon' l_{2_f} = 8 \rightarrow 6f\varepsilon l_{2_f} = 9$ and $6f\varepsilon' l_{2_f} = 10 \rightarrow 6f\varepsilon l_{2_f} = 9$ for $L_f = 12$. The element $|S_{ij}|^2$ of the short-range scattering probability matrix gives the probability that an electron in channel j will scatter into channel i in a single collision with the core. Two channels $i \neq j$ are said to be strongly coupled if the corresponding element of the scattering probability matrix $|S_{ij}|^2$ is large. For the process $6g\varepsilon' l_{2_f} = 8 \rightarrow 6f\varepsilon l_{2_f} = 9$ the scattering probability matrix element is 0.26, whereas for $6g\varepsilon' l_{2_f} = 10 \rightarrow 6f\varepsilon l_{2_f} = 9$ the matrix element is 0.07. This verifies the usual propensity rule that the outermost electron tends to gain angular momentum as well as energy when it autoionizes.

For the $L_f = 6$ calculation the propensity-favored decay $6g\varepsilon' l_{2_f} = 8 \rightarrow 6f\varepsilon l_{2_f} = 9$ occurs with a probability of 0.046. This is approximately one fourth of the probability for the propensity-favored decay probability for $L_f = 12$, which explains why the Rydberg series converging to the $6g$ threshold is much broader in the $L_f = 12$ calculation of Fig. 2. The larger coupling for the $L_f = 12$ calculation can be explained by examining the $1/r_{12}$ matrix element. For strongly interacting channels i and j the matrix element $\langle i|1/r_{12}|j\rangle$ will be large. Comparing the dipole part of the angular matrix element for $L_f = 12$ and $L_f = 6$ we find

$$\langle (fl_{2_f} = 9)L_f = 6|1/r_{12}|(gl_{2_f} = 8)L_f = 6\rangle = 0.057, \quad (21)$$

$$\langle (fl_{2_f} = 9)L_f = 12|1/r_{12}|(gl_{2_f} = 8)L_f = 12\rangle = 0.46. \quad (22)$$

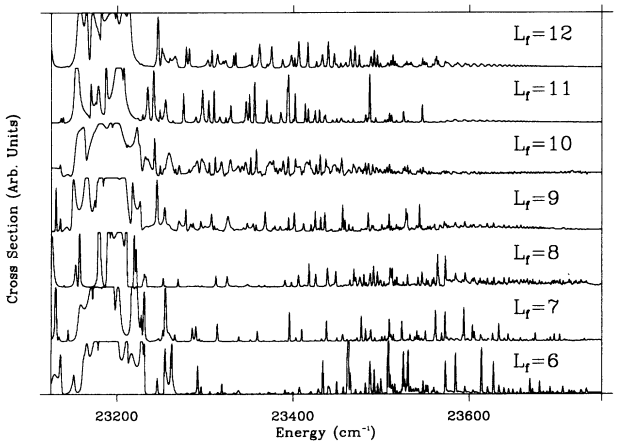

FIG. 2. The calculated partial cross sections for the individual L_f. Only one L_i is plotted for each L_f because cross sections with the same L_f but different L_i have the same resonance positions, only the intensities differ.

B. Photoionization cross section of barium

In this section we apply the formalism developed in Sec. II to the photoionization cross section of barium. We will be considering the two-photon excitation of excited barium using the isolated-core approximation. The isolated-core approximation assumes that the inner core electron absorbs a photon while the outer electron is a spectator. Here we will extend the usual isolated-core approximation to treat the case of two-photon excitation.

We will consider photoionization from the excited $6s_{1/2}n_il_i$ initial states to final states in the energy region near the $8s_{1/2}$ threshold. Experimental cross sections have been measured by Camus *et. al.* [6] by a two-photon isolated-core excitation. In the isolated-core excitation, the outer electron is excited to a high Rydberg Stark state lying in a hydrogenic manifold just below the $Ba^+(6s)$ state, in the presence of an electric field. The field is then adiabatically reduced to leave the atom in a specific l_i angular momentum eigenstate. The orbital angular momentum of the initial state can be mixed if there are stray electric fields in the experiment, an effect observed by Ref. [19]. After the atom has been excited to the high-n_il_i state the ionizing laser excites the core electron by a two-photon process.

In the isolated-core approximation the transition amplitude is written as a product of an amplitude to excite the core electron and of an overlap factor for the outer electron, as in Eq. (16). The specific form for the core-electron transition amplitude in a two-photon process is different from the one-photon amplitude discussed for strontium. The transition amplitude to excite a final core state $|f\rangle$ from an initial state $|i\rangle$ by a two-photon process can be written in general as

$$D = \sum_j \frac{\langle f|\hat{\varepsilon}\cdot\mathbf{r}|j\rangle\langle j|\hat{\varepsilon}\cdot\mathbf{r}|i\rangle}{E_j - E_i - \hbar\omega}. \quad (23)$$

The sum is taken over all intermediate states $|j\rangle$ coupled to the initial state by the dipole operator $\hat{\varepsilon}\cdot\mathbf{r}$. The energy denominator contains the initial state energy E_i, the intermediate state energy E_j, and the photon energy $\hbar\omega$.

For an initial ionic s state having $l_i = 0$, dipole selection rules limit the intermediate state to be a p state with $l_j = 1$. The possible final state angular momenta are then $l_f = 0, 2$. For the small energy region we will be considering, approximately 300 cm^{-1}, we will neglect the

energy dependence of the denominator in Eq. (23). This is valid because there are no intermediate ionic states $|j\rangle$ with orbital angular momentum $l_j = 1$ near the energy $E_i + \hbar\omega$, but it would fail of course, if there was an intermediate p state which could be resonantly excited. The transition amplitude can be written as a sum of irreducible tensorial operators having rank 0 and rank 2

$$D = D^{(0)} + D^{(2)}. \tag{24}$$

The rank 0 operator $D^{(0)}$ causes $s \rightarrow s$ ionic transitions, while the rank 2 operator $D^{(2)}$ causes $s \rightarrow d$ transitions.

We now make a further approximation to neglect the $D^{(2)}$ part of the two-photon transition amplitude, which is primarily justified by the fact that the ionizing laser frequency is close to half of the $6s \rightarrow 8s$ transition frequency and far from any $6s \rightarrow nd$ frequency. Moreover, in the isolated-core approximation the analytical form for the overlap of the outer electron wave function Eq. (18) falls off rapidly for large differences in the effective quantum number $\nu_f \neq \nu_i$. Here ν_f is the effective quantum number of the final state at an energy E, i.e., $\nu_f = 1/\sqrt{2(E_f - E)}$ with E_f the threshold energy. The factor ν_i is the effective quantum number of the initial state and is equal to the principal quantum number $\nu_i = n_0$. In the experiment of Ref. [6] final states were probed in the energy region near effective quantum numbers of $\nu_f = 12 - 16$ relative to the $8s_{1/2}$ threshold at $E_{8s_{1/2}} = 58\,025.18$. The nearest d threshold is the $7d_{3/2}$ ionic state at $E_{7d_{5/2}} = 59\,800.31$, and the effective quantum number relative to the $7d_{3/2}$ at these energies is in the range 6–7. The $T^{(2)}$ amplitude for direct excitation of the $7d_{3/2}$ channels is thus also weak owing to the large difference between their effective quantum numbers from that of the initial state.

The resulting approximation to the reduced transition amplitude, from the initial state MQDT wave function $\Psi_i = \Phi_i(\Omega)u_{n_i l_i}$ to the final state MQDT wave function $\Psi_\beta = \sum_j \Phi_j(\Omega)[f_j(r_2)I_{j\beta} - g_j(r_2)J_{j\beta}]$, with $\Phi_j(\Omega)$ having the form given in Eq. (6), reads

$$D_\beta = \langle \Psi_\beta || D^{(0)} || \Phi_i \rangle \tag{25}$$

$$\cong \sum_j \langle \Phi_j || D^{(0)} || \Phi_i \rangle \int_{r_0}^{\infty} dr_2 u_{n_i l_i}(r_2)[f_j(r_2)I_{j\beta} - g_j(r_2)J_{j\beta}] + D_\beta^{\text{inside}}. \tag{26}$$

This expression neglects exchange and all correlation effects in the *initial* state. D_β^{inside} is the contribution to the transition amplitude from inside of the reaction volume. The sum in Eq. (26) is taken over all final state channels included in the calculation. The choice of channels to include will be discussed in the next section along with the comparison between experiment and theory.

The reduced matrix element $\langle \Phi_j || D^{(0)} || \Phi_i \rangle$ in jK coupling is

$$\langle \Phi_j || D^{(0)} || \Phi_i \rangle = C \delta_{l_{1_i} l_{1_f}} \delta_{l_{2_i} l_{2_f}} \delta_{j_{1_i} j_{1_f}} \delta_{K_i K_f}. \tag{27}$$

Here the constant C is the reduced matrix element of the rank 0 operator $D^{(0)}$ between the initial and final state ionic radial functions. We do not need to calculate this integral because experiments to date have measured only the relative cross sections.

Figure 3 displays the relative photoionization cross section measured by Ref. [6], while Fig. 4 shows our calculation. The calculations were performed in jK coupling with an R-matrix box of 100 a.u. Numerical tests showed that it was unnecessary to propagate the solutions outside of the reaction volume, in contrast to the Sr calculation. The final state core levels included in the calculation as open or weakly closed are

$$8s_{1/2}, 7p_{1/2,3/2}, 8p_{1/2,3/2}, 6d_{3/2,5/2}, 7d_{3/2,5/2},$$
$$4f_{5/2,7/2}, 5f_{5/2,7/2}, 5g_{7/2,9/2}. \tag{28}$$

The final state channels were constructed from these core levels by adding an outer electron of orbital angular l_{2_f}, satisfying the condition that $\mathbf{K}_f = \boldsymbol{l}_{2_f} + \mathbf{j}_{2_f}$. The theoretical cross section contains 2000 energy mesh points over an energy region from 57 200 to 57 640 cm^{-1} above the first ionization potential.

The energy scale in Fig. 3 and Fig. 4 is relative to the $6s_{1/2} \rightarrow 8s_{1/2}$ ionic transition. These figures show the evolution of the final state interaction as a function of the initial state outer electron orbital angular momentum l_{2_i} for $n_{2_i} = 13$. The experimental (Fig. 3) cross section shows some contamination of neighboring l_{2_f} peaks due to stray electric fields in the apparatus [19]. In jK coupling for $j = 1/2$ there are two possible K_i values for each l_{2_i}, $K_i = l_{2_i} - 1/2, l_{2_i} + 1/2$. The calculated cross section is a sum of the two possible K_i. For sufficiently high l_{2_i} a single peak occurs in the cross section because the resonance positions for the two K_f values are degenerate.

A dramatic change occurs in the experimental cross section for the case of $l_{2_i} = 7$. The complex structure in the experimental cross section is not reproduced in the theoretical calculation where we see two simple peaks split by the K-splitting . The complex structure in the experiment can be identified to be due to Rydberg series converging to the $5f_{5/2}$ and $5f_{7/2}$ thresholds. This discrepancy is not fully understood, however it is possible that there is a perturber from one of the $7d_j$ thresholds which is in the wrong position in the calculation. The cross section would depend sensitively on the position of the perturber because the interaction between the $8s_{1/2}l_2 = 7$ channel and the $5f_j l'_2$ channels can be enhanced through an intermediate d perturber. This effect has been observed in the cross section for $l_{2_i} = 6$ and is discussed below. Another possibility is that the experimental cross section has a large fraction of $l_{2_i} = 6$ mixed in due to the stray electric fields. Comparing the $l_{2_i} = 7$ and $l_{2_i} = 8$ experimental cross sections in Fig. 3 it is clear that there is a large fraction of the $l_{2_i} = 8$ charac-

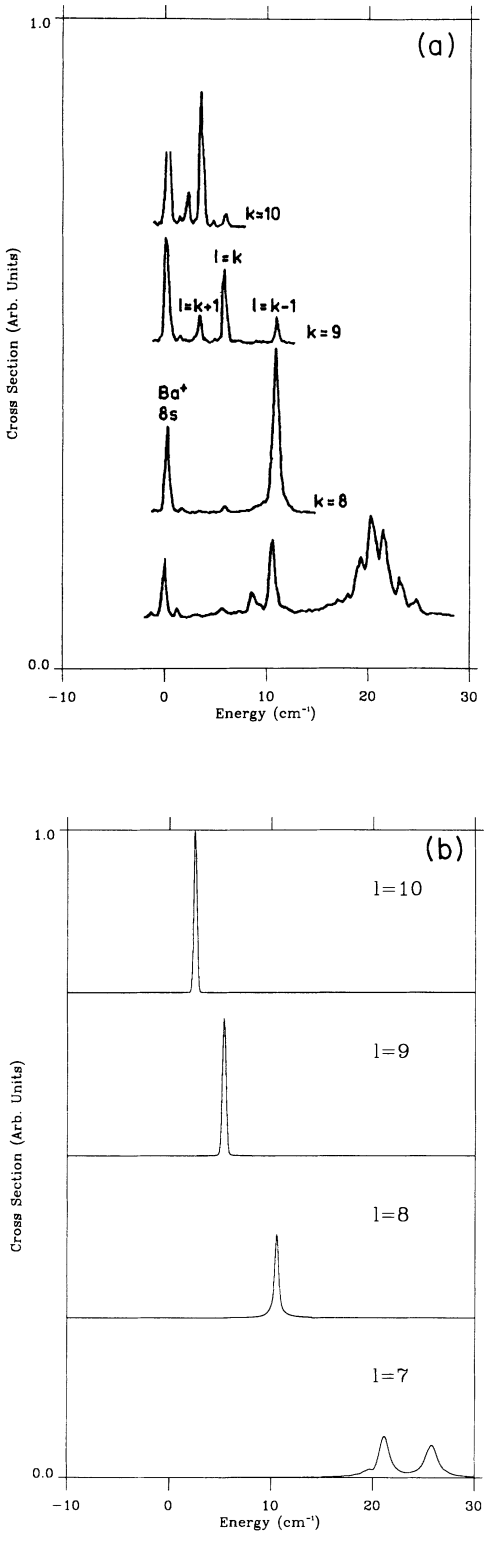

FIG. 3. (a) Experimental relative cross section plotted as a function of energy relative to the $6s_{1/2} \rightarrow 8s_{1/2}$ ionic transition energy. (From Ref. [7].) The plots are labeled for different l_{2_f}, the outer electron orbital angular momentum. (b) Theoretical relative cross section plotted as a function of energy relative to the $6s_{1/2} \rightarrow 8s_{1/2}$ ionic transition energy. The plots are labeled for different l_{2_f}, the outer electron orbital angular momentum.

ter present in the $l_{2_i} = 7$ spectrum near 10 cm^{-1}. Also, there is a structure in the $l_{2_i} = 6$ cross section similar to that in the $l_{2_i} = 7$ cross section near 20 cm^{-1}.

In Fig. 4 we display the experimental and theoretical cross section for the initial state $n_{2_i} = 14 l_{2_i} = 6$ over a much larger energy region, including the overlap structure from $\nu_{8s} = 16 \rightarrow \nu_{8s} = 12$. The overlapping resonances are due to the $5f_j \varepsilon' l'_2$ channels, with the $5f_{5/2}$ threshold at -0.1061 a.u. and the $5f_{7/2}$ threshold at -0.105 a.u. One very noticeable discrepancy between experiment and theory is in the intensities of the $5f_j \varepsilon l_{2_f}$ series. For energies in the range -0.1056 to -0.1062 a.u. the experimental $5f_j \varepsilon l_{2_f}$ resonances all have approximately the same intensity, while the theoretical cross section over the same energy range follows the distribution of the squared overlap integral given in Eq. (24). Two possible explanations for the discrepancy between experiment and theory are as follows. Firstly the approximation we have made to the dipole matrix elements discussed above could be overly simplified. This is currently difficult to test because the full calculation for the two-photon process is beyond our present capabilities. The second possible explanation which we have examined is the presence of a perturber in the energy region of Fig. 4.

In order to examine the possible effects of a perturber in the energy region of Fig. 4 we have examined the energy derivative of the eigenphase sum which contains information about the resonance positions but does not incorporate the transition amplitude. Figures 5(a) and Fig. 6(a) display the individual K contributions to the theoretical cross section of Fig. 4. Figures 5(b) and 6(b) display the derivative of the eigenphase sum for three cases: (1) treating the $8s_{1/2} \varepsilon l_2, 7d_j \varepsilon l_2$ and $5f_j \varepsilon l_2$ channels as open [denoted sdf-open in Figs. 5(b), 6(b)], (2) treating the $8s_{1/2} \varepsilon l_2$ and $5f_j \varepsilon l_2$ channels as open (denoted sf-open), and (3) treating the $5f_j \varepsilon l_2$ channels as open (denoted f-open). Artificially opening a channel in the MQDT calculation removes all perturbers associated

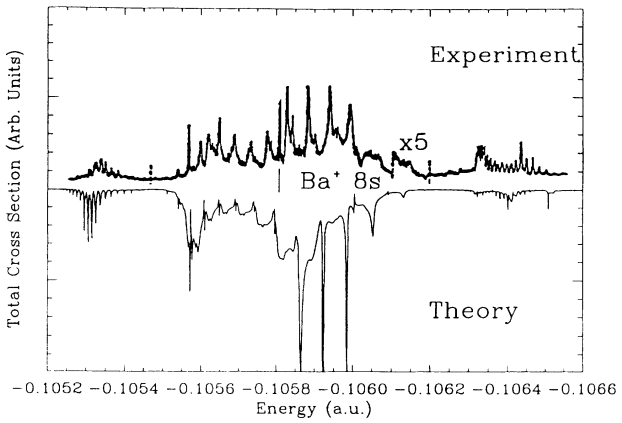

FIG. 4. Comparison of the experimental relative cross section (top, from Ref. [7]) with the theoretical cross section (bottom) for the initial state $n_{2_i} = 14, l_{2_i} = 6$. The theoretical cross section is shown as a mirror image for comparison. The position of the Ba^+ ionic line is labeled for reference.

with that channel. In Fig. 5(b) the calculation denoted sdf-open has a perturber at approximately -0.106 a.u. which must be of $5g_j nd$ character, because all other channels which could contribute a perturber in this energy range have been treated as open in the MQDT calculation. Similarly, in the $K^\pi = 11/2^+$ calculation [Fig. 6(b)] with the $7d_j \varepsilon l_2$ channels treated as closed (denoted sf-open) there is an additional perturber at -0.1054 a.u. in the $K^\pi = 11/2^+$ symmetry and at $-0.106\,05$ a.u. in the $K^\pi = 13/2^+$ symmetry. These perturbers must be of $7d_j ng$ character. From an examination of the eigenphase sum with the $5f_{7/2}\varepsilon l_2$ channels treated as closed we have determined that the effect of the $5g_j nd$ perturber in the $K^\pi = 11/2^+$ calculation is to narrow the $5f_j nl_2$ resonances. This can be seen in Fig. 5(a) where the resonances in the vicinity of the $5g_j nd$ perturber have reduced widths. The $5g_j nd$ perturber in the $K^\pi = 13/2^+$ symmetry [Fig. 6(a)] is near the minimum of the ICE overlap factor and therefore has little effect on the spectra. In both the $K^\pi = 11/2^+$ and $K^\pi = 13/2^+$ symmetries the effect of the $7d_j ng$ perturber on the widths of the $5f_{7/2}n_2 l_2$ resonances appears to be minimal. However, as will be seen below, the $7d\varepsilon l_2$ channels play a crucial role in determining the intensity of these resonances.

It is very surprising that the intensities of the $5f_j \varepsilon l'_{2_f}$ series are so large, in view of the fact that mixing of the $8s\varepsilon l_{2_f} = 6$ channel with the $5f_j \varepsilon' l'_{2_f}$ channels requires a change of three units of angular momentum. This led Camus *et al.* [6] to speculate that these channels are strongly coupled by the octopole component of $1/r_{12}$, which our analysis below appears not to substantiate.

We can qualitatively understand the complexity of the spectra for different l_{2_f} by looking at the adiabatic potentials. Shown in Fig. 7 are the eigenvalues of the matrix $E_i\delta_{ij} + V_{ij}(r_2)$ plotted as a function of the square root of the outer electron radial coordinate r_2, with V_{ij} given by Eq. (11). The plots labeled (a)–(f) are for different values of the outer electron orbital angular momentum $8sl'$ and quantum numbers K^π_f, with π the parity of the state. The $8s_{1/2}\varepsilon l_{2_f}$ channel is the single potential curve labeled in the figures. The $5f_{5/2}\varepsilon' l'$ and $5f_{7/2}\varepsilon' l'$ channels lie energetically directly below the $8s$ channel at large r_2. It is clear in figures (c)–(f) that the single potential labeled $8sl$ in each figure is almost completely diabatic, which indicates that the interaction with the neighboring channels is small. Due to the small channel interactions we expect the photoionization spectra to be simple for $l_{2_i} = 7, 8$. This is true in the theoretical calculation of the cross section in Fig. 4. However, in the experimental spectra in Fig. 3 the $l_{2_i} = 8$ cross section is simple while the $l_{2_i} = 7$ cross section is very complex. As discussed above, the complexity in the experimental $l_{2_i} = 7$ spectra may be due to mixing of the $l_{2_i} = 7$ state with the $l_{2_i} = 6$ state by stray electric fields.

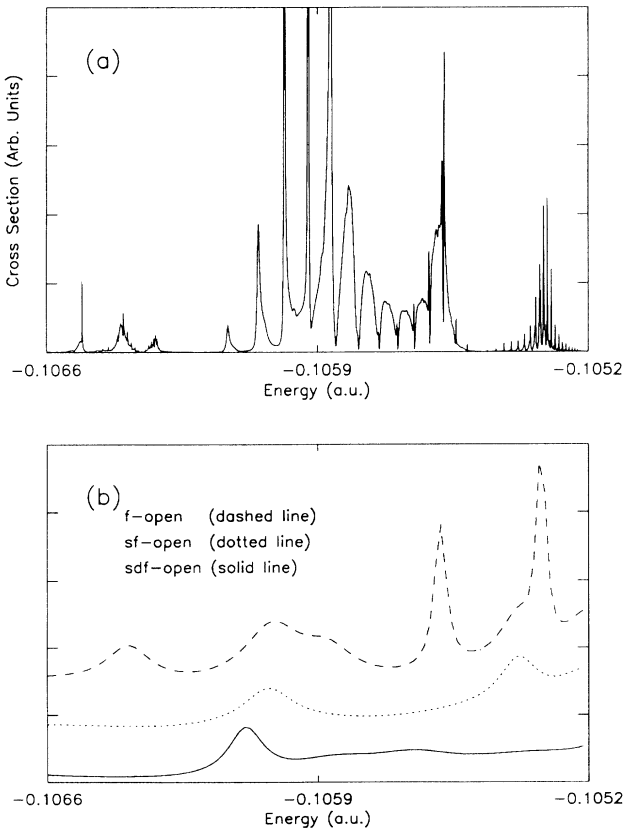

FIG. 5. (a) The calculated cross section for the $K^\pi = 11/2^+$ symmetry and (b) the derivative of the eigenphase sum. The three curves in (b) are explained in the text.

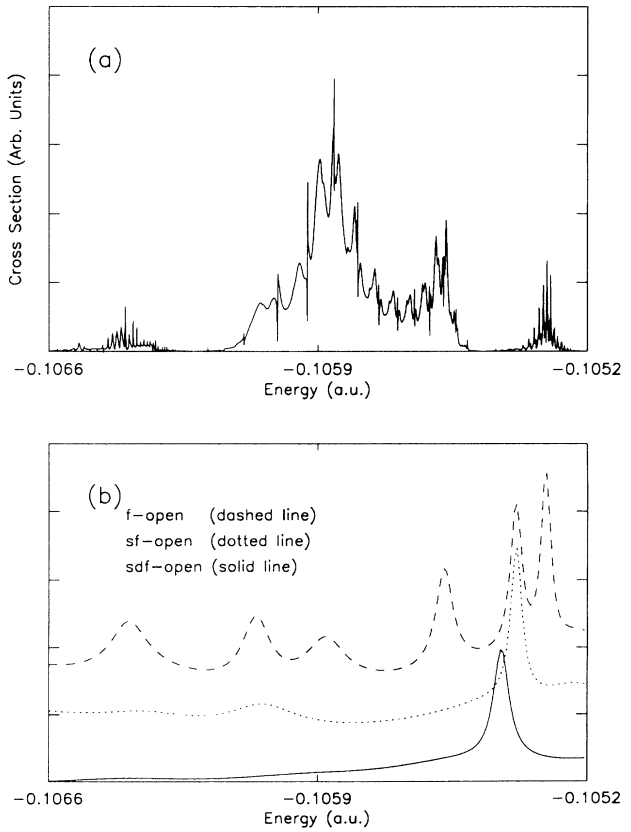

FIG. 6. (a) The calculated cross section for the $K^\pi = 13/2^+$ symmetry and (b) the derivative of the eigenphase sum. The three curves in (b) are explained in the text.

The interactions in the adiabatic potentials become much stronger in Figs. 7(a) and 7(b). In Fig. 7(a) there is a large avoided crossing between the $5f_{5/2}l_{2_f} = 7$ potential and the $7d_{3/2}l_{2_f} = 6$ potential at small radial distances which we suspect is responsible for the large intensity of the resonances converging to the $5f_j$ thresholds in Fig. 4. However, the large number of avoided crossings between many of the channels makes it difficult to sort out the exact mechanism responsible for the coupling between the $8s_{1/2}\varepsilon l_{2_f} = 6$ channel and the $5f_j\varepsilon' l'_{2_f}$ channels solely from an examination of the adiabatic potentials and eigenvectors. To quantitatively understand the strength of the $5f_j$ series and to specify the exact mechanism responsible for the coupling it is necessary to examine the scattering probability matrix.

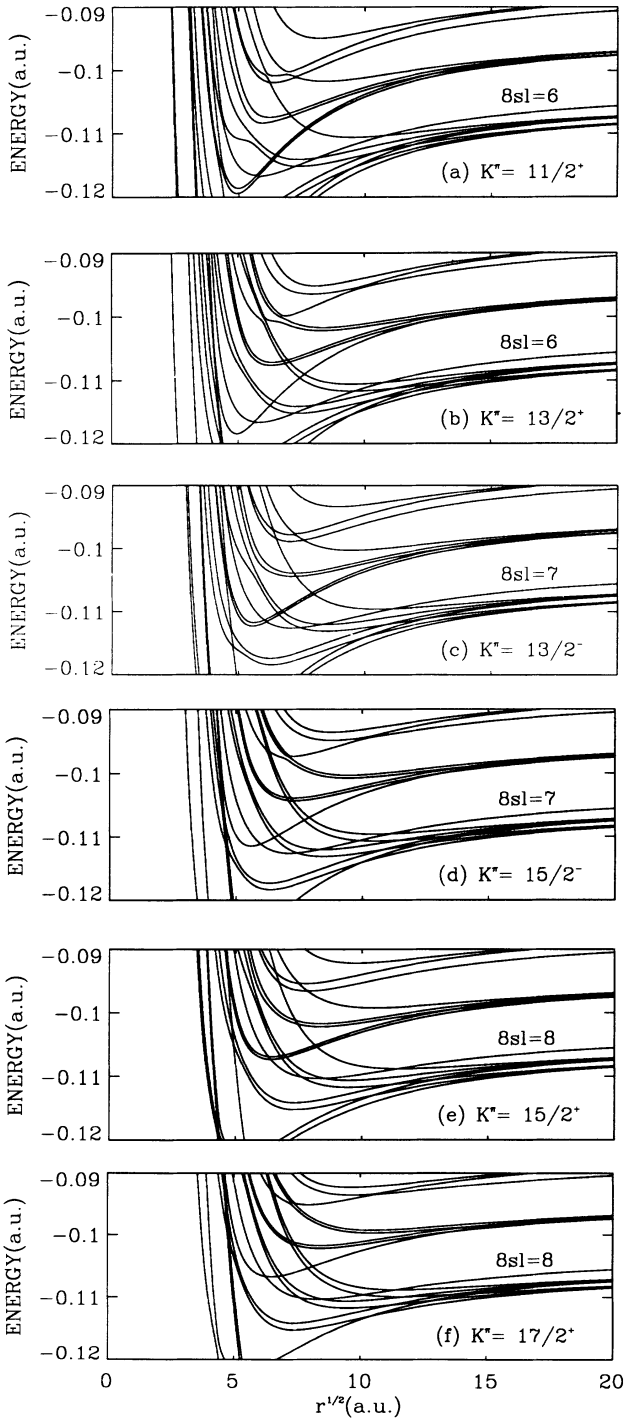

FIG. 7. Barium adiabatic potential curves for outer electron angular momentum $l_{2_f} = 6 - 8$ plotted as a function of the square root of r_2, with r_2 the outer electron radial coordinate. The quantum numbers K and π are discussed in the text.

We will now discuss the specific mechanism responsible for the interaction between the $8s_{1/2}\varepsilon l_{2_f} = 6$ channel and the $5f_j\varepsilon' l'_{2_f}$ channels. We have calculated the weakly energy dependent scattering probability matrix $|S_{ij}|^2$ with an R-matrix box size of $r_0 = 50$ a.u. and analyzed the elements connecting the $8s_{1/2}\varepsilon l_{2_f} = 2$ channel to the $5f_j\varepsilon' l_{2_f}$ channels at an energy of -0.1058. The largest coupling was found for the $5f_{7/2}\varepsilon l_{2_f} = 7$ channel. A Rydberg electron striking the core in the $8s_{1/2}\varepsilon l_{2_f} = 6$ channel scatters into the $5f_{7/2}\varepsilon l_{2_f} = 7$ channel with a probability of 0.16. However, if we treat the $7d_j\varepsilon l_{2_f}$ channels in the MQDT calculation as if they were open, the scattering probability decreases to 0.046. This dramatic decrease in the scattering probability provides strong evidence that the interaction between the $8s_{1/2}\varepsilon l_{2_f} = 6$ and $5f_j\varepsilon' l_{2_f}$ channels is being mediated through an interaction with the $7d_j\varepsilon'' l''_{2_f}$ channels. To rule out the possibility that the interaction between the $8s_{1/2}\varepsilon l_{2_f} = 6$ channel and the $5f_{7/2}\varepsilon' l_{2_f} = 7$ channel is due to a direct octopole coupling we repeated the calculation of the scattering probability matrix omitting all multipoles higher than $k = 2$ in the expansion of $1/r_{12}$. The scattering probability with the $7d_j\varepsilon'' l''_{2_f}$ channels treated as closed in the MQDT calculation was found to be 0.14, and with the $7d_j l\varepsilon'' l''_{2_f}$ channels treated as open, 0.045. This is a relatively small difference from the calculation including all multipoles, again providing strong evidence that the strong coupling between these two channels is being mediated by an interaction with one of the $7d_j\varepsilon l_{2_f}$ channels and is not due to direct octopole coupling.

IV. CONCLUSIONS

We have presented a general theoretical framework that provides a detailed interpretation of high-lying asymmetric two-electron states. Treatment of long-range multipole interactions has been included by propagation of the R-matrix solutions to large radial distances where the application of standard MQDT is possible.

Application of this procedure to treat photoionization of highly excited Sr and Ba has shown that despite the complexity of the spectra the effect of the channel interactions can be sorted out by examining "smooth" quantities of MQDT (such as the scattering probability matrix). Examination of the scattering probability matrix for Ba photoionization has allowed us to interpret the complexity of the spectra observed experimentally in [7]. We find that the coupling between the $8sl = 6$ channel and the $5f_j l_{2_f}$ channels is a two-step process, mediated by the $7d_j l'_{2_f}$ channels, and not direct octopole coupling as suggested by Ref. [6]. While the $k = 1$ (dipole) and $k = 2$ (quadrupole) multipoles are important, octopole

coupling plays a relatively minor role.

These kind of experiments provide a handle on an interesting class of two-electron states, in which the electrons exhibit nonperturbative correlations despite the fact that they are almost completely nonoverlapping. Given the extreme complexity of these experiments, and the considerable uncertainty about the preparation of the state being photoionized, the present calculations account for the measurements of Refs. [5,6] reasonably well. The calculations also show far richer substructure not resolved by Refs. [5,6], which shows that future experimental studies at higher resolution are desirable.

ACKNOWLEDGMENTS

We thank U. Eichmann and W. Sander for providing us with their numerical data. We are grateful to P. Camus for providing us with photoionization cross section data prior to publication, and for informative discussions. We would also like to thank F. Robicheaux for many helpful discussions regarding the calculations. This research is supported by the Division of Chemical Sciences, Office of Basic Energy Sciences, Office of Energy Research, U.S. Department of Energy Grant No. DE-FG-02-90ER14145.

[1] M. Domke, C. Xue, A. Puschmann, T. Mandel, E. Hudson, D. A. Shirley, G. Kaindl, C. H. Greene, H. R. Sadeghpour, and H. Peterson, Phys. Rev. Lett. **66**, 1306 (1991).

[2] J. -Z. Tang, S. Watanabe, M. Matsuzawa, and C. D. Lin, Phys. Rev. Lett. **69**, 1633 (1992).

[3] H. R. Sadeghpour and C. H. Greene, Phys. Rev. Lett. **65**, 313 (1990).

[4] P. G. Harris, H. C. Bryant, A. H. Mohagheghi, R. A. Reeder, H. Sharifian, H. Tootoonchi, C. Y. Tang, J. B. Donahue, C. R. Quick, D. C. Risloue, and W. W. Smith, Phys. Rev. Lett. **65**, 309 (1990).

[5] U. Eichmann, V. Lange, and W. Sandner, Phys. Rev. Lett. **68**, 21 (1992).

[6] P. Camus, S. Cohen, L. Pruvost, and A. Bolovinos, Phys. Rev. A **48**, R9 (1993).

[7] C. H. Greene and M. Aymar, Phys. Rev. A **44**, 6271 (1991).

[8] U. Fano and A. R. P. Rau, *Atomic Collisions and Spectra* (Academic, Orlando, FL, 1986), p. 69.

[9] M. Gailitis and R. Damburg, Proc. Phys. Soc. London **82**, 192 (1963).

[10] H. R. Sadeghpour and M. Cavagnero, J. Phys. B **26**, L271 (1993); H. R. Sadeghpour, C. H. Greene, and M. Cavagnero, Phys. Rev. A **45**, 1587 (1992).

[11] Francis Robicheaux and C. H. Greene, Phys. Rev. A **47**, 4908 (1993).

[12] Francis Robicheaux and C. H. Greene, Phys. Rev. A **48**, 4429 (1993).

[13] C. H. Greene, Phys. Rev. A **42**, 1405 (1990).

[14] C. H. Greene and L. Kim, Phys. Rev. A **38**, 5953 (1988).

[15] C. H. Greene and Ch. Jungen, Adv. At. Mol. Phys. **21**, 51 (1985).

[16] W. E. Cooke, S. A. Bhatti, and C. L. Cromer, Opt. Lett. **7**, 69 (1982).

[17] M. D. Lindsay, C.-J. Dai, L.-T. Cai, T. F. Gallagher, F. Robicheaux, and C. H. Greene, Phys. Rev. A **46**, 3789 (1992).

[18] R. N. Zare, *Angular Momentum* (Wiley, New York, 1988).

[19] P. Camus, C. R. Mahon, and L. Pruvost, J. Phys. B: At. Mol. Opt. Phys. **26**, 221 (1993).